NMR Studies of Water Transport and Proton Exchange in Water-in-Carbon Dioxide Microemulsions

Kaz Nagashima,[†] C. Ted Lee, Jr.,[‡] Bin Xu,[†] Keith P. Johnston,[‡] Joseph M. DeSimone,[†,§] and Charles S. Johnson, Jr.*[,†]

Department of Chemistry, University of North Carolina, Chapel Hill, North Carolina 27599, Department of Chemical Engineering, University of Texas at Austin, Austin, Texas, 78712, and Department of Chemical Engineering, North Carolina State University, Raleigh, North Carolina 27695

Received: October 21, 2002

Water-in-carbon dioxide (W/C) microemulsions stabilized by an ammonium carboxylate perfluoropolyether ($PFPECOO^-NH_4^+$) surfactant are studied with NMR diffusion and relaxation methods with the aim of obtaining information on the dynamics of this system, as well as aiding in the design of new surfactants that can form stable microemulsions in CO_2. Short proton transverse relaxation times (3−10 ms) measured for water and ammonium ions are shown to agree with a simple proton exchange model. As the pressure is lowered below the phase boundary, the NMR spectra indicate that surfactant migrates to the new liquid phase along with the water. Diffusion coefficients are reported in the CO_2 density range of 0.88−1.00 g/mL at 25 °C. The fractional amounts of water diffusion in bulk CO_2, within the droplets, and through the water channels are delineated quantitatively. In decreasing the density from 0.96 to 0.88 g/mL, the water diffusion coefficient increases by a factor of 2 while the diffusion coefficients for ammonium ions and $PFPECOO^-$ remain approximately constant. The droplet clusters are formed with channels that permit water molecules to diffuse freely over distances on the order of microns. This detailed dynamic molecular description of these clusters complements, in a consistent manner, macroscopic studies of percolation by conductivity measurements and equilibrium measurements of correlation lengths by SANS.

Introduction

Liquid or supercritical carbon dioxide (CO_2) is a nontoxic and nonflammable solvent that is especially attractive in manufacturing and cleaning operations because of solvation properties that are tunable with pressure. Furthermore, the readily accessible critical conditions (T_c = 31 °C, P_c = 73.8 bar) and low heat of vaporization of CO_2 lead to economical and energy-efficient recovery of solutes. Applications are, however, limited by the inability of CO_2 to dissolve many lipophilic and hydrophilic compounds. It is, therefore, extremely important to form water-in-CO_2 (W/C) microemulsions that have the ability to dissolve both polar and hydrophobic solutes. These microemulsions provide environmentally benign replacements for organic solvents as media for reactions between polar and nonpolar molecules and for separation and purification processes.

The commercially available ammonium carboxylate perfluoropolyether surfactant ($PFPECOO^-NH_4^+$) with molar mass approximately 700 g/mol has been shown to form W/C microemulsions at modest pressures (100−200 bar, 35−60 °C) with water-to-surfactant mole ratios (W_o) up to 30.[1,2] Small-angle neutron scattering (SANS) studies reveal the existence of spherical water droplets with radii 20−35 Å,[2,3] and various spectroscopic methods including FTIR of D_2O and visible absorption of the probe molecule methyl orange indicate the presence of aggregated water domains.[1,4] Furthermore, conductivity measurements suggest the aggregation of microemulsion droplets and thus percolation as the volume fraction of droplets increases.[5]

In this work, we apply ^1H and ^{19}F NMR diffusion and relaxation measurements to investigate dynamics in (W/C) microemulsions containing $PFPECOO^-NH_4^+$. In contrast to the methods mentioned above, resolved NMR signals permit transport properties to be measured for all of the chemical species present. From the outset we know this is an extremely complicated system. Water molecules are dissolved in CO_2 as well as existing in various states of binding inside the micelles,[4] and we expect that there is rapid exchange between these sites. Similarly, the surfactant exists in solution as unimers, in the microemulsion droplets, and in droplet aggregates with possible surfactant exchange taking place. Here single surfactant molecules are referred to as unimers rather than monomers since they themselves are oligomeric. Finally, protons exchange between water and ammonium ions, and ammonia may be present in micelles and in the bulk CO_2. We use relaxation times (T_2) to demonstrate the proton exchange reaction and the diffusion coefficients to determine the hydrodynamic radius of the micelles and the mobilities of water and ammonium ions. Water diffusion data are compared with conductivity measurements and correlation lengths from previous SANS experiments to assess the aggregation of droplets and possible onset of percolation. The NMR data will be shown to provide substantial insight into the dynamic behavior of these microemulsions beyond what could be gained from macroscopic conductivity measurements. In particular, the mobility of water and the

* Author to whom correspondence should be addressed. Phone: (919) 966-5229. Fax: (919) 843-6041. E-mail: charles_johnson@unc.edu.
[†] University of North Carolina.
[‡] University of Texas at Austin.
[§] North Carolina State University.

10.1021/jp0222705 CCC: $25.00
Published on Web 02/06/2003

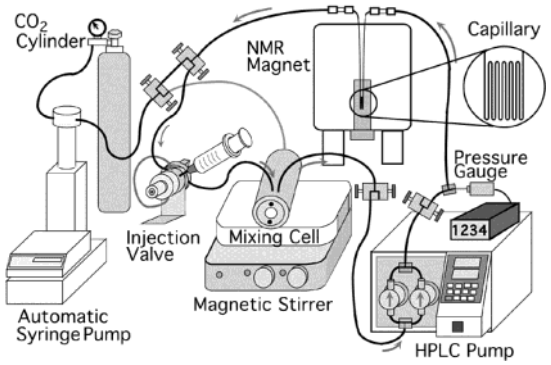

Figure 1. Experimental apparatus for high-pressure NMR experiments.

ammonium ion are distinguished from that of the surfactant, supporting realistic molecular models.

Experimental Section

Materials. An ammonium carboxylate perfluoropolyether surfactant

$$CF_3-(O-CF_2-CF(CF_3))_n-O-CF_2-COO^-NH_4^+$$

was used in all experiments (abbreviated $PFPECOO^-NH_4^+$). The surfactant had an average molecular weight of 676 g/mol ($n \sim 2.9$) and was synthesized from the acid form (Ausimont, Lot # 3610 RB) as previously described.[5] SFC/SFE grade CO_2 (Air Products, >99.9999%) and distilled water were used throughout.

Microemulsion Phase Behavior and Electrical Conductivity. The microemulsions were prepared in a high-pressure, variable-volume view cell equipped with a sapphire window that permitted visual observation of microemulsion formation and phase behavior.[6] A piston inside the view cell was used to vary the pressure independently of temperature. System pressure was controlled with a syringe pump (Isco, model 260D) to within 1 bar by using CO_2 as the pressurizing fluid on the backside of the piston. The cell contents were mixed with a magnetic stir bar inside the cell. The microemulsion cloud point at each concentration was measured by decreasing the pressure from 450 bar until the clear, one-phase microemulsion became cloudy. Conductivity measurements were performed as described previously.[5]

High-Pressure NMR. The experimental apparatus for high-pressure NMR is illustrated in Figure 1. All of the microemulsion studies were performed with a fused-silica capillary (Polymicro Technologies, 150 μm i.d. × 360 μm o.d.) for the NMR cell.[7] As previously noted, the capillaries safely withstand high pressures while stabilizing the low viscosity samples against mass convection.[8] Twelve turns were folded in 7 cm segments using a micro torch equipped with a disposable butane lighter. The bare ends of the exposed capillary were recoated with cyanoacrylate glue, and the resulting flame-folded capillary had a pressure rating of ca. 500 bar. Microemulsions were prepared in the phase-behavior cell mentioned above and circulated through the capillary with an HPLC pump (Waters) at the flow rate of 5 mL/min. A six-port, two-position valve (Valco) equipped with a 200 μL sample loop was used to incrementally add water to the system. Acetone-d_6 (Cambridge Isotope) was flame-sealed into a 1.5 mm o.d. glass capillary and inserted into a 5 mm NMR tube in parallel with the high-pressure capillary for use as an external reference.

NMR measurements were performed with a Bruker Avance 500 spectrometer operated at 500.13 MHz for proton (^{1}H) and 470.55 MHz for fluorine (^{19}F) observations. The detection region of a 5 mm Nalorac diffusion probe was calibrated to 25.0 ± 0.1 °C with a thermocouple. One-dimensional NMR spectra were obtained with a single 20° pulse and a 15 s relaxation delay. For ^{1}H spectra, 16k data points were typically acquired for 20 ppm (1000 Hz) of spectral width, and 64 transients were accumulated to achieve satisfactory signal-to-noise ratios (S/N) (ca. 20/1 for the NH_4^+ resonance). The free induction decays were zero-filled to twice of acquired data points (32k) after exponential line-broadening of 10 Hz. The resonances were integrated after automatic polynomial baseline correction with the xwinnmr program (Bruker, version 2.6) to suppress a broad resonance from the polyimide coating of capillary. The bipolar pair longitudinal eddy current delay (BPP-LED) sequence was used for the diffusion measurements (acquisition time = 0.41 s, relaxation delay = 1 s, gradient pulse width δ = 1 ms, separation in BPP τ = 1 ms, diffusion time scale typically Δ = 5 ms, longitudinal eddy current delay T_e = 200 μs, 64 transients accumulated after 32 steady-state dummy scans).[9] The diffusion coefficients were then obtained by nonlinear regression with the following equation:

$$S(q) = S(0)\exp\left[-Dq^2\left(\Delta - \frac{\delta}{3} - \frac{\tau}{2}\right)\right] \qquad (1)$$

where $S(q)$ is the signal intensity, $q = \gamma g \delta$, γ is the gyromagnetic ratio, and g is the gradient amplitude (0 to 1.03 *T/m*). For the ^{19}F signals, plots of $\ln[S(q)]$ vs q showed increasing curvature as Δ was stepped from 12.5 ms to 100 ms. This may indicate a unimer ↔ micelle exchange process for the surfactant, but the changes are too small to permit analysis, and we have minimized the effect by using Δ = 5 ms for the reported diffusion coefficients.

The longitudinal relaxation times (T_1) were measured with a conventional inversion recovery sequence. The apparent transverse relaxation times for H_2O and NH_4^+ protons were estimated from line widths in the one-dimensional spectra.

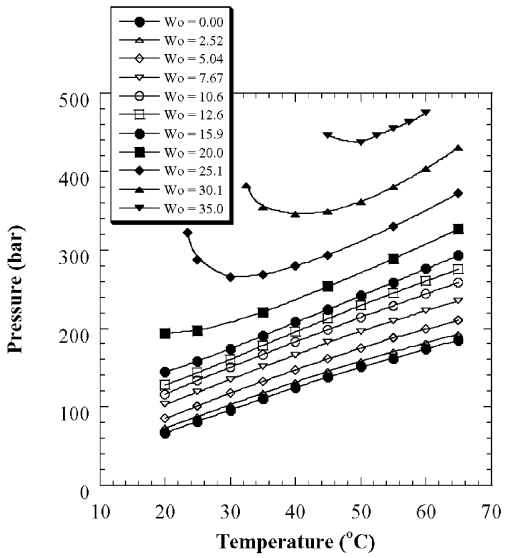

Figure 2. Phase behavior of water/$PFPECOO^-NH_4^+$/CO_2 microemulsions as a function of W_o at [S/C] = 0.012.

Results and Discussion

Phase Behavior. Microemulsion phase-behavior data as a function of the water-to-surfactant mole ratio W_o, corrected for the solubility of water in CO_2,[10] are presented in Figure 2 at a surfactant-to-CO_2 molar ratio of [S/C] = 0.012. One-phase

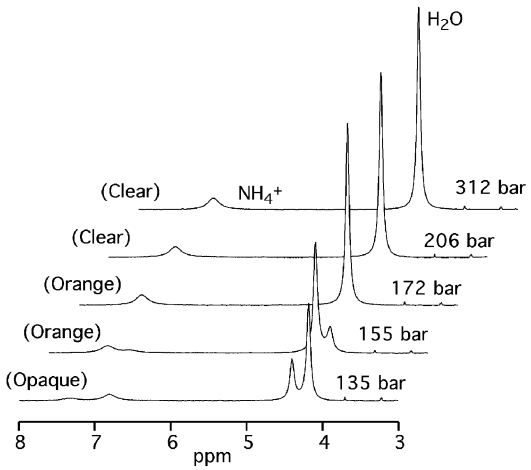

Figure 3. ^{1}H NMR spectra at various pressures for [S/C] = 0.0137 and W_o = 10.4 at 25 °C, revealing the formation of droplet clusters below 172 bar and phase separation at 132 bar.

regions are found above each curve, while two phases exist below each curve. The composition and nature of these phases depend on the type of the phase transition. The parts of each cloud-point curve with a positive slope on the $P-T$ diagram have been shown to be a result of droplet−droplet interactions, and the two phases that result upon phase separation are both microemulsion phases, one rich and one lean in droplet concentration.[3,5,11] A negative slope on the cloud-point curve indicates a phase transition resulting from changes in the curvature of the interface, giving rise to a microemulsion phase and an essentially pure water phase beyond the cloud point. In the present study the pressure was changed at constant temperature; therefore, lowering the pressure resulted in the system approaching the droplet-interaction-type phase transition. Near the cloud point, droplet interactions result in the formation of clusters of droplets with aggregated sizes that are large enough to scatter light. This gives rise to the solutions exhibiting a slight orange tinge (when viewed at small scattering angles) at pressures just above the cloud point. The solutions became opaque within seconds of crossing the phase boundary, followed by phase separation into a top (clear) phase and bottom (deep orange) phase of roughly equal volumes, again indicating droplet interactions.

NMR Spectra, T_2 Relaxation, and Proton Exchange. ^{1}H NMR spectra (Figure 3) of microemulsion mixtures at W_o = 10.4 in the single-phase region show NH_4^+ and H_2O signals at approximately 7.0 and 4.3 ppm, respectively, relative to TMS. The ratio of the integrals of the H_2O and NH_4^+ signals approximates $W_o/2$ but must be corrected for the solubility of H_2O in CO_2. As the pressure is reduced, new NH_4^+ and H_2O signals appear on the low frequency side (right side) of the original peaks. These correspond to the droplet-rich phase described above, and they continue to grow at the expense of signals from the droplet lean phase. The difference in the magnetic susceptibilities of the two phases is responsible for the frequency shifts in the pairs of peaks.[12] The NMR spectra show clearly that surfactant precipitates along with the water droplets during phase separation. This type of phase separation is often caused by interdroplet interactions. The measurements of diffusion coefficients below provide detailed insight into the dynamics of these interations. The other primary type of phase separation is expulsion of pure water without surfactant from the microemulsion droplet due to a change in the curvature of the interface. Clearly the NMR spectra indicate that this mechanism is not operative. The ability to discriminate between phase separation mechanisms is useful for designing new surfactants, especially in choosing surfactant tails to mediate interdroplet interactions. Furthermore, NMR may be utilized to investigate opaque phase-separated systems that are difficult to analyze with light scattering.

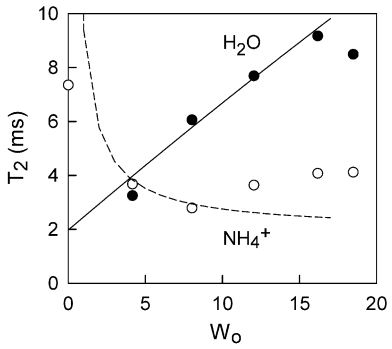

Figure 4. ^{1}H transverse relaxation times (T_2) versus W_o for water and ammonium ions at P = 270 bar showing the dominating effect of proton exchange on relaxation times and hence line widths.

These ^{1}H signals show considerable broadening, and the approximate T_2 values (Figure 4) can be obtained with the eq $1/T_2 = \pi\Delta\nu_{1/2}$ where $\Delta\nu_{1/2}$ is the full width at half-height. The spin−lattice relaxation times T_1 and the diffusion coefficients were also measured for the ^{1}H and ^{19}F signals. These values were found to depend on both the recirculation time and the time lapse before measurements were made. Samples with W_o = 8.4 were recirculated for 20 min and this was repeated up to four times. Also, the elapsed time between the termination of recirculation and the initiation of measurements was varied from zero to 600 min.

Circulation through the folded capillary tube results in restricted flow through the multiple bends and exerts shear forces on the microemulsion that may cause structural changes. We found that the proton T_1 values decrease from 500 to 350 ms for a total recirculation time of 80 min, while the T_2 values and diffusion coefficients (D) remain relatively constant. Also, T_1 values are dependent on the time lapse between recirculation and measurement. The trend is downward, but the values typically remain above 330 ms. Again, T_2 and D values are relatively independent of the elapsed time. It appears that circulation disrupts the microemulsion structure, perhaps homogenizing the mixture, and a new equilibrium is only slowly attained. The relaxation times and D values for ^{19}F signals in the CF_3 region of the spectrum were less dependent on recirculation time and on the time lapse before measurement. T_1 remained in the range 1.0 to 1.1 s and T_2 fluctuated between 280 ms and 320 ms with recirculation time from zero to 80 min. However, D did begin to increase after 40 min of recirculation

Figure 4 illustrates the small proton T_2 values and their strong dependence on W_o at 25 °C and 276 bar. This sample was prepared with 2.02 g of $PFPECOO^-NH_4^+$ and 10.0 g of CO_2 (10.3 mL of CO_2 added to the cell at 21 °C and 276 bar) to give droplet volume fractions of $\phi = \phi_{water} + \phi_{surfactant} = 0.098$ to 0.17 over this W_o range. Usually, the dominant relaxation mechanism for protons is provided by the magnetic dipole−dipole interaction. The relaxation rates $R_1 = 1/T_1$ and $R_2 = 1/T_2$ resulting from dipole−dipole interactions depend on the correlation times for molecular reorientation and collisions. Typically, T_1 and T_2 in low viscosity fluids are long (>100 ms), and slow motions, e.g., the rotation of a large droplet, are indicated when $T_2 < T_1$. However, the very small values of T_2 found in this study are not consistent with reasonable correlation times.

This fact and the strong dependence of the T_2 values on W_o suggest a proton exchange process.

Studies by Grunwald et al. of ammonium ions in aqueous solutions reveal a variety of mechanisms for exchange of protons between H_2O and NH_4^+.[13,14] The inverse micelles in our microemulsion mixture have radii of about 3 nm, and their aqueous core (pH = 3)[15] is approximately $(55/W_o)$ M in ammonium ions. The important exchange reactions for this system are

$$NH_4^+ + H_2O \underset{k_{-4}}{\overset{k_4}{\rightleftharpoons}} NH_3 + H_3O^+ \quad (2)$$

and

$$H_3\overset{+}{N}H + NH_3 \xrightarrow{k_6} H_3N + H\overset{+}{N}H_3 \quad (3)$$

We note that the ammonium ion signal in Figure 3 is a singlet even though the J_{NH} coupling in the ammonium ion is approximately 53 Hz.[16] This is consistent with line narrowing by the rapid proton exchange described by eq 3, and the slow exchange reaction described by eq 2 provides a model for the W_o-dependent T_2 values shown in Figure 4. However, the exchange rates are much higher than those found in aqueous solutions of ammonium ions and reflect binding states and restricted motion inside the inverse micelles. The T_1 relaxation rate of the ^{14}N nucleus may also be reduced in this environment, but this has not been confirmed. Deuteron exchange in aqueous solutions of $PFPECOO^-NH_4^+$ salts has previously been reported.[17]

To interpret the observed line widths, we adopt the simple two-site model of proton exchange.[18] Since the line widths are much less than the frequency separation of the peaks, this is the slow exchange limit where the exchange contribution to the transverse relaxation rate for the ith peak is given by $R_{2i} = 1/\tau_i$ where τ_i is the mean lifetime of a proton in the ith site. Here "site" means a location where the proton has a definite chemical shift, i.e. attached to oxygen or to nitrogen. The transverse relaxation rates can be written as

$$R_2^i = \left(\frac{1}{T_2^i}\right)_0 + \frac{1}{\tau_i} \quad (4)$$

where the first term on the right-hand side represents the relaxation rate in the absence of exchange. In the following, $A = [H_2O]$ and $B = [NH_4^+]$ where the concentrations refer to the cores of the microemulsion droplets and $W_o = A/B$. The fractions of protons in sites A and B are given by $P_A = W_o/(W_o + 2)$ and $P_B = 2/(W_o + 2)$, respectively, taking into account the statistical factors; and we define τ as the meantime between exchange events. In an exchange event, a proton randomly selects any available site including the one it occupies, i.e., two A sites and four B sites for six distinct possibilities. This analysis assumes that $k_{-4} \gg k_4$ so that τ is determined by k_4. With these definitions the mean lifetimes are given by $\tau_A = \tau/P_B = 2/(k_4B)$ and $\tau_B = \tau/P_A = 4/(k_4A)$. In computing the solid and dashed curves in Figure 5 we have approximated T_2 values in the absence of exchange by the measured T_1 values and have replaced W_o with fW_o where f ($\sim$0.5) is an adjustable parameter to account for the fraction of water molecules that are available for proton exchange. The fits obtained confirm the basic validity of the proton exchange model; but, of course, this simple model neglects important details such as the nonuniform distribution of ammonium ions and the nature of water binding to surfactant headgroups.

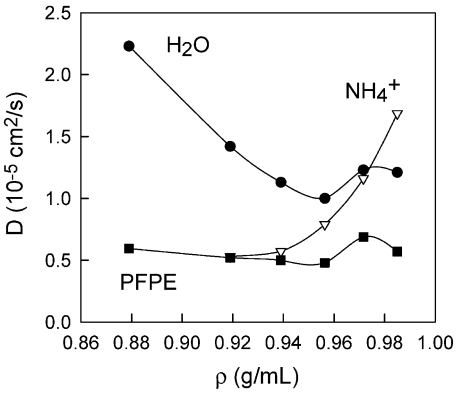

Figure 5. Diffusion coefficients (D) for water, NH_4^+, and the surfactant versus CO_2 density (ρ) with $W_o = 8.4$. The increase of the water diffusion coefficient with decreasing density provides clear evidence of droplet clustering.

Diffusion Measurements. The diffusion coefficients of water, counterion, and surfactant are shown in Figure 5 as functions of CO_2 density. Lowering the density results in an initial decrease followed by a sharp increase in the diffusion coefficient of water. This phenomenon is also observed, albeit to a weaker extent, in the diffusion coefficient of the surfactant.

Lowering the density and, hence, solvent power of CO_2 has been shown to result in an increase in droplet interactions through a strong surfactant tail−tail force that develops, resulting in the formation of droplet clusters.[3,5,11] The initial decrease in the diffusion coefficients of water and surfactant is consistent with the formation of clusters of droplets that diffuse more slowly than single droplets due to their larger aggregated size. Further decreases in CO_2 density result in an increase in the average number of droplets per cluster, allowing for the rapid transport of water molecules via transient water channels that develop between droplets in a cluster.

The large values of the diffusion coefficient of water obtained at the lowest density, approaching the self-diffusion coefficient of pure water (2.29×10^{-9} m^2/s),[19] are an indication of a high degree of clustering in the microemulsion. The root-mean-square distance a water molecule moves during an observation time of Δ can be estimated by $\langle r^2\rangle^{1/2} = \sqrt{6D\Delta}$. Thus, for an observation time of 5 ms, $\langle r^2\rangle^{1/2} = 8 \times 10^{-6}$ m, indicating that micron-sized clusters would have to develop in order to produce the observed increase in the diffusion coefficient measured by NMR at low densities.

To analyze the diffusion-coefficient data in Figure 5, care must be taken to account for each possible mechanism of water motion. Water can reside in three locations in the W/C microemulsion, namely inside the water droplets, in bulk CO_2, or in the water channels that develop between clustered droplets. We assume the fast exchange limit so that the measured diffusion coefficient of water is a weighted sum of the diffusion coefficients of water in each location and is given by[20−22]

$$D = p_D D_D + p_{CO_2} D_{CO_2} + p_{channel} D_{channel} \quad (5)$$

where p_D, p_{CO_2}, and $p_{channel}$ are the fractions of the time Δ that a water molecule spends in droplets, in bulk CO_2, and in the transient water channels, and D_D, D_{CO2}, and $D_{channel}$ are the diffusion coefficients for water in each location, respectively.

As an estimate of the diffusion coefficient of the droplets (D_D), the diffusion coefficient of the surfactant is used. Note that no correction needs to be made for molecularly dissolved surfactant in CO_2 because the critical microemulsion concentra-

tion ($c\mu c$) of this surfactant in CO_2, which is approximately the concentration of molecularly dissolved surfactant in CO_2, is very low (0.019 wt %)[23] compared to the overall surfactant concentration (16.7 wt %). The hydrodynamic radius, R_H, of the droplet can be estimated from D_D by means of the corrected Stokes−Einstein equation for tracer diffusion $D_D = k_BT(1 - \alpha\phi)/(6\pi\eta R_H)$ where ϕ is the droplet volume fraction, $\alpha \approx 2$ for hard spheres,[24] and η is the viscosity of CO_2. We estimate that $\phi = 0.13$ from the composition of the mixture and the densities of water (1 g/mL), $PFPECOO^-NH_4^+$ (1.8 g/mL), and CO_2 (0.915 g/mL). From the data in Figure 5 at 200 bar and 25 °C ($\eta = 0.098$ cP), $D_D = 4.8 \times 10^{-10}$ m^2/s, thus we calculate that $R_H = 3.4$ nm. This number agrees quite well with the sum of the core radius (2 nm) and surfactant tail length (1.3 nm) obtained from SANS.[3]

With R_H and the reported headgroup area $a_H = 76$ Å^2 at 25 °C,[23] it is possible to obtain an independent estimate of the volume fraction. For a core radius of $R_c = R_H - l_t$ where l_t is the length of the surfactant tail, we can obtain estimates of both the surface area S_c ($= 4\pi R_c^2$) and the total micellar volume V_m ($= 4\pi R_H^3/3$). The number of surfactant molecules per micelle is given by $N_s = S_c/a_H$, and this permits the total number of micelles N_m to be determined. To obtain the droplet volume fraction ϕ, we note that the surfactant tails are solvated by a substantial amount of CO_2; thus, the total micelle volume calculated above includes the volume of this solvating CO_2. Therefore, we can obtain $\phi = N_m V'_m/V$, where V is the volume of the sample calculated by assuming ideal mixing, and $V'_m = 4\pi R_H^3/3 - nN_s v_{CO_2}$, with n equal to the number of CO_2 molecules solvating each surfactant tail and v_{CO_2} equal to the molecular volume of CO_2 at the given density ($= 79.9$ Å^3). Assuming $n = 18$, similar to the value estimated from the scattering length density contrast measured with SANS,[2,3] this procedure gives $\phi = 0.12$, in excellent agreement with the value calculated above directly from the mixture composition and component densities. Furthermore, W_o can be estimated from the molecular volume of water $v_w = 30$ Å^3 and the radius of the *water* core (R_W), i.e., the radius of the core minus the thickness of the surfactant ion layer (~ 4.5 Å) with the equation $W_o = 4\pi R_w^3/(3v_w N_s)$. This gives a value of $W_o = 8.6$, again in excellent agreement with the value calculated above from the mixture composition. Together, the agreements obtained in the calculated values of ϕ and W_o support the accuracy of the value obtained in this study for the droplet diffusion coefficient (D_D).

For the fraction of water molecularly dissolved in CO_2, we assume that CO_2 is saturated with water,[4,11] and recent NMR measurements give D_{CO_2} as a function of pressure at 25 °C.[25] To obtain the diffusion coefficient of water through the channels, we assume that at the lowest density studied droplet-cluster size diverges (see below) and, therefore, the diffusion of these large clusters can be ignored. Thus, at the lowest density, diffusion is due to water in the channels and in bulk CO_2 only, giving a value of $D_{channel} = 1.79 \times 10^{-9}$ m^2/s.

With these assumptions, the relative fraction of water in each location can be calculated from eq 5 as shown in Figure 6. Note that as the density is decreased, a larger percentage of the water diffuses through the water channels, while the fraction of water diffusing with the droplets decreases. In other words, as the droplet clusters become large the distance a water molecule can diffuse inside the cluster, which is given by $\langle r^2\rangle^{1/2}$ as discussed above increases, and this diffusion becomes measurable during the time scale of NMR experiments.

The relative contribution of each diffusion pathway to the overall diffusion coefficient, namely p_iD_i, is shown in Figure 7. Again, as density is lowered, diffusion through the growing channels, which is expected to be fast, begins to dominate the overall diffusion process. Furthermore, as density is decreased, the diffusion due to water diffusing with the droplets decreases as a result of the decrease in the diffusion rate of the growing droplet clusters. Note that although the water dissolved in CO_2 is only around 3% of the total water in the system, the contribution due to the diffusion of water in CO_2 is large, ranging from 20 to 40%, due to the low viscosity ($\sim$0.1 cP) and resulting in high diffusivities observed in near-critical CO_2. Also, $p_{CO_2}D_{CO_2}$ is fairly constant due to the fact that both the solubility of water in CO_2 and the viscosity of CO_2 vary little over the density range employed.

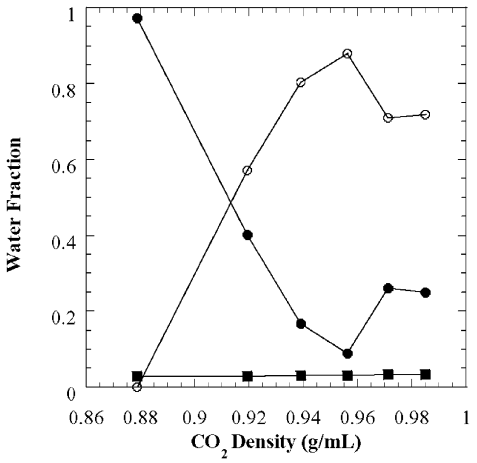

Figure 6. Fraction of water diffusing in CO_2 (■), with the droplets- (○), and through water channels (●).

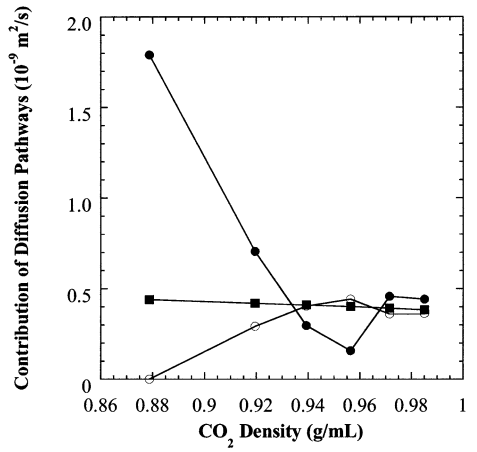

Figure 7. Magnitude of the contribution of each diffusion mechanism p_iD_i with $i = CO_2$, droplets, and H_2O to the overall diffusion of water as a function of the density of CO_2. Symbols are the same as in Figure 6.

Additional comments are necessary concerning the density dependence of diffusion coefficients for $PFPECOO^-$ and NH_4^+ shown in Figure 5. We suggest that the behavior of the surfactant is similar to that of AOT in the water−AOT−decane microemulsions as the percolation threshold is crossed by increasing the temperature.[20] Beginning at the highest density the diffusion coefficient of $PFPECOO^-$ is constant or decreases slightly as clusters begin to form on decreasing the density because the clusters diffuse slower than individual droplets. However, as the clusters continue to grow, diffusion of the surfactant across the surface of the cluster results in an increase in the diffusion coefficient of $PFPECOO^-$. These two combined effects result

in a weak minimum in the diffusion coefficient of $PFPECOO^-$ versus density.

Up to a CO_2 density of about 0.94 g/mL, NH_4^+ is localized in the water core and moves with the droplet. In fact, NH_4^+ is unaffected by the formation of water channels, indicating a strong association with surfactant headgroups. The increase in the diffusion coefficient of NH_4^+ at higher densities is more difficult to explain. A possible explanation is suggested by eq 2 where NH_3 is shown to be in equilibrium with NH_4^+. If NH_3 partitions into the CO_2 phase, the average diffusion coefficient measured for the protons attached to nitrogen would be expected to increase. The diffusion coefficient of NH_3 in CO_2 would be expected to be large and similar in size to that of H_2O in CO_2, so even a low concentration would contribute significantly to the average. While the increased partitioning of a small quantity of NH_3 into the CO_2 phase as pressure is increased in the NH_3/CO_2/water system is a well-known phenomenon at these conditions,[26] independent evidence concerning the partitioning of NH_3 into CO_2 in the water/$PFPECOO^-NH_4^+$/CO_2 system is not available.

Conductivity Measurements. To further support the claim that droplet clustering is responsible for the sharp increase in the diffusion coefficient of water at low densities, it is useful to examine microemulsion electrical-conductivity and SANS data. Conductivity data are useful as a measure of the transport properties over the same millisecond time scale as used in NMR,[27] while SANS data can be used as a direct measurement of droplet interactions and clustering.[28−30]

From Figure 6 it is shown that water diffuses equally with the droplets and between the water channels at a density of around 0.91 g/mL. It has been shown in the water/AOT/decane microemulsion system that this equality occurs at the percolation threshold temperature, i.e., the temperature at which an "infinite" cluster forms as a result of increasing the temperature and, thus, droplet interactions.[20] For the water/$PFPECO^-NH_4^+$/CO_2 system, the percolation volume fraction, i.e., the volume fraction at which an "infinite" cluster forms at a given T and P, was found to be $\phi = 0.16$ at 25 °C and $P = 200$ bar ($\rho = 0.915$ g/mL).[5] In the present study $\phi = 0.13$, indicating that the system should be close to the percolation threshold at $\rho = 0.91$ g/mL, as was obtained from Figure 6. This agreement with regard to the proximity to the percolation threshold between the NMR diffusion coefficient and electrical-conductivity data supports the claim of the effect of droplet clusters on water transport.

Further support for this argument can be gained by reconsidering Figure 6, specifically the minimum observed at approximately 0.96 g/mL in the contribution of water diffusion through channels in comparison with Figure 8, which is a plot of the normalized microemulsion electrical conductivity σ/ϕ and the correlation length ξ determined from neutron scattering.[3] The correlation length is a measure of the scale at which the microemulsion is macroscopically homogeneous[31] and, hence, can be thought of as a rough measure of cluster size. Both σ/ϕ and ξ go through a minimum at a density of around 0.97 kg/L, similar to the NMR data in Figures 6 and 7. This indicates that droplet interactions and cluster formation are minimized at a density of around 0.96−0.97 kg/L. This has been rationalized by an increase in surfactant tail−tail interactions as the density of CO_2 is either decreased *or* increased from this minimum. The increase in droplet interactions as CO_2 density is increased results from CO_2 becoming too good of a solvent for the PFPE surfactant tail at higher densities.[3,5,11] For example, the solubility parameter of CO_2 is 18.4 $(MPa)^{1/2}$ at 25 °C and 345 bar, while the solubility parameter of PFPE is 10.4 $(MPa)^{1/2}$.[32] Also note

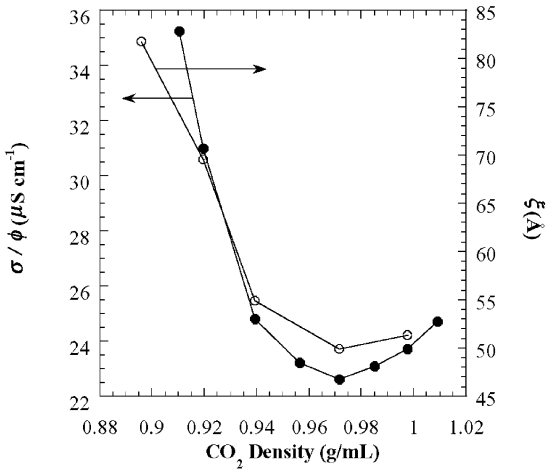

Figure 8. Normalized microemulsion conductivity σ (●) and the correlation length ξ (○) from SANS.

in Figure 8 that the correlation length and, thus, cluster size, diverges at a density of 0.91 g/mL, consistent with the value obtained in Figure 6 for the density at which an "infinite" cluster forms.

Conclusions

We have demonstrated the use of NMR spectroscopy including diffusion and relaxation measurements to obtain molecular-level details about the structure and dynamics of W/C microemulsions. The measurements of transverse relaxation times as a function of W_o for water and ammonium protons show the presence of proton exchanges between oxygen and nitrogen sites. Also, the proton spectra reveal rapid water-mediated proton exchange between ammonium ions. These results are consistent with the very high, nonuniform concentrations of ammonium ions found near the droplet interface.

In addition, NMR diffusion measurements provide hydrodynamic radii for microemulsion droplets that are consistent with core radii from SANS and the known fluorocarbon tail lengths. The droplet volumes, surface areas, hydrodynamic radii, and volume fractions all agree with the previously reported headgroup area for $PFPECOO^-$. The proton spectra clearly reveal the separation of the microemulsion into droplet-rich and droplet-lean phases as the optically observed cloud point is traversed by means of decreasing CO_2 density. With decreasing CO_2 density, the water diffusion coefficient first decreases and then strongly increases with the formation of droplet clusters at low CO_2 density. The droplet clusters are formed with channels that permit water molecules to diffuse freely over distances on the order of microns. The diffusion coefficient of the surfactant increases at low density as the surfactant is able to migrate along the cluster surface. This detailed dynamic molecular description of these clusters complements, in a consistent manner, macroscopic studies of percolation by conductivity measurements and equilibrium measurements of correlation lengths by SANS.

The emerging understanding of the structure and dynamics of these droplets, including droplet phase separation due to attractive interdroplet interactions, will be highly useful for designing new surfactants to form stable microemulsions in CO_2.

Acknowledgment. This work was supported under NSF Grant CHE-9903723 (C.S.J.) and by the STC program of the NSF under agreement CHE-9876674.

References and Notes

(1) Johnston, K. P.; Harrison, K. L.; Clarke, M. J.; Howdle, S. M.; Heitz, M. P.; Bright, F. V.; Carlier, C.; Randolph, T. W. *Science* **1996**, *271*, 624−626.

(2) Zielinski, R. G.; Kline, S. R.; Kaler, E. W.; Rosov, N. *Langmuir* **1997**, *13*, 3934−3937.

(3) Lee, C. T.; Johnston, K. P.; Dai, H. J.; Cochran, H. D.; Melnichenko, Y. B.; Wignall, G. D. *J. Phys. Chem. B* **2001**, *105*, 3540−3548.

(4) Clarke, M. J.; Harrison, K. L.; Johnston, K. P.; Howdle, S. M. *J. Am. Chem. Soc.* **1997**, *119*, 6399−6406.

(5) Lee, C. T.; Bhargava, P.; Johnston, K. P. *J. Phys. Chem. B* **2000**, *104*, 4448−4456.

(6) Lee, C. T.; Psathas, P. A.; Johnston, K. P.; deGrazia, J.; Randolph, T. W. *Langmuir* **1999**, *15*, 6781−6791.

(7) Yonker, C. R.; Zemanian, T. S.; Wallen, S. L.; Linehan, J. C.; Franz, J. A. *J. Magn. Reson. A* **1995**, *113*, 102−107.

(8) Cain, J. B.; Zhang, K.; Betts, D. E.; DeSimone, J. M.; Johnson, C. S., Jr. *J. Am. Chem. Soc.* **1998**, *120*, 9390−9391.

(9) Wu, D.; Chen, A.; Johnson, C. S., Jr. *J. Magn. Reson. A* **1995**, *115*, 260−264.

(10) Wiebe, R. *Chem. Rev.* **1941**, *29*, 475−481.

(11) Lee, C. T.; Johnston, K. P.; Dai, H. J.; Cochran, H. D.; Melnichenko, Y. B.; Wignall, G. D. *J. Phys. Chem. B* **2002**, *104*, 11094−11102.

(12) Dardin, A.; Cain, J. B.; DeSimone, J. M.; Johnson, C. S., Jr.; Samulski, E. T. *Macromolecules* **1997**, *30*, 3593−3599.

(13) Grunwald, E.; Karabatsos, P. J.; Kromhout, R. A.; Purlee, E. L. *J. Chem. Phys.* **1960**, *33*, 556−563.

(14) Emerson, M. T.; Grunwald, E.; Kromhout, R. A. *J. Chem. Phys.* **1960**, *133*, 547−555.

(15) Niemeyer, E. D.; Bright, F. V. *J. Phys. Chem. B* **1998**, *102*, 1474−1478.

(16) Fraenkel, G.; Asahi, Y.; Batiz-Hernandez, H.; Bernheim, R. A. *J. Chem. Phys.* **1966**, *44*, 4647−4649.

(17) Beekakker, C. W. J.; Mazur. *Physica A* **1984**, *126*, 349.

(18) Johnson, C. S., Jr. Chemical Rate Processes and Magnetic Resonance. In *Advances in Magnetic Resonance, Vol. 1*; Waugh, J. S., ed.; Academic Press: New York, 1965; pp 33−102.

(19) Mills, R. *J. Phys. Chem.* **1973**, *77*, 685−688.

(20) Arkhipov, V. P.; Idiyatullin, Z. S.; Arkhipov, R. V.; Zakharchenko, N. L.; Zuev, Y. F.; Fedotov, V. D. *Colloid J.* (*Engl. Tr.*) **2000**, *62*, 407−413.

(21) Stilbs, P. *Prog. NMR Spectrosc.* **1987**, *19*, 1−45.

(22) Johnson, C. S., Jr. *J. Magn. Reson. A* **1993**, *102*, 214−218.

(23) daRocha, S. R.; Johnston, K. P. *Langmuir* **2000**, *16*, 3690−3695.

(24) Schmitz, K. S. *An Introduction to Dynamic Light Scattering by Macromolecules*; Academic Press: Boston, 1990; Chapter 6.

(25) Xu, B.; DeSimone, J. M.; Johnson, C. S., Jr. *J. Phys. Chem. A* **2003**, *107*, 1−3.

(26) Lemkowitz, S. M.; van Erp, J. C.; Rekers, D. M.; van der Berg, P. J. *J. Chem. Biotechnol.* **1980**, *30*, 85−101.

(27) Caboi, F.; Capuzzi, G.; Baglioni, P.; Monduzzi, M. *J. Phys. Chem. B* **1997**, *101*, 10205−10212.

(28) Kotlarchyk, M.; Chen, S.-H.; Huang, J. S. *Phys. Rev. A* **1983**, *28*, 508−511.

(29) Huang, J. S.; Safran, S. A.; Kim, M. W.; Grest, G. S.; Kotlarchyk, M.; Quirke, N. *Phys. Rev. Lett.* **2002**, *53*, 592−595.

(30) Chen, S. H. *Annu. Rev. Phys. Chem.* **1986**, *37*, 351−399.

(31) Knackstedt, M. A.; Ninham, B. W.; Monduzzi, M. *Phys. Rev. Lett.* **1995**, *75*, 653−656.

(32) Lawson, D. D. *Appl. Energy* **1980**, *6*, 241−255.